3D-printed Perforated Trailing Edges for Broadband Noise Abatement

Rubio Carpio, Alejandro; Avallone, Francesco; Ragni, Daniele; Snellen, Mirjam; van der Zwaag, Sybrand

DOI
10.2514/6.2019-2458

Publication date
2019

Document Version
Final published version

Published in
25th AIAA/CEAS Aeroacoustics Conference

Aeroacoustics Conferences
20-23 May 2019, Delft, The Netherlands
25th AIAA/CEAS Aeroacoustics Conference

10.2514/6.2019-2458

3D-printed Perforated Trailing Edges for Broadband Noise Abatement

Alejandro Rubio Carpio *, Francesco Avallone †, Daniele Ragni ‡, Mirjam Snellen § and Sybrand van der Zwaag ¶
Delft University of Technology, Delft, The Netherlands, 2629HS

Turbulent boundary layer trailing-edge noise scattered by a NACA0018 airfoil equipped with 3D printed perforated trailing-edge inserts, i.e. with straight cylindrical channels connecting the two sides of the airfoil, is investigated. The inserts have different permeability in order to assess the effect of this property on broadband noise generation. Far-field noise is measured with a phased microphone array. The experiments are performed at free-stream velocities of 26 and 41 m/s, corresponding to chord-based Reynolds numbers of 3.4×10^5 and 5.4×10^5, and at angles of attack of 0 and 4.8°. The inserts, with permeability values of 1.5×10^{-9} and 5.4×10^{-9} m^2, attenuate respectively up to 5 and 9.5 dB at 0° and up to 4 and 7.5 dB at 4.8° incidence. The noise abatement of inserts with straight passages is compared with that of inserts manufactured using metallic foams with a random pore distribution but similar permeability. It is found that to achieve similar overall noise attenuation levels, the perforated inserts require at least 3 times higher permeability than the metal foam inserts. From this we conclude that in order to maximize the noise attenuation potential of permeable inserts, the inner structure of the permeable trailing-edge insert must be considered.

I. Nomenclature

α	=	angle of attack , degree
δ^*	=	displacement thickness, m
C	=	form drag coefficient, m^{-1}
c	=	chord, m
c_0	=	speed of sound, m s^{-1}
d_h	=	hole diameter of the perforated inserts, m
D	=	diameter of the phased microphone array, m
Δf	=	frequency resolution, Hz
f	=	frequency, Hz
f_s	=	sampling frequency, Hz
l_h	=	hole spacing of the perforated inserts, m
L	=	span, m
$L_{p\ (1/3)}$	=	sound pressure level in one-third octave bands, dB
μ	=	dynamic viscosity, N s m^{-2}
n_b	=	number of sampled points within a data block
$\overline{p^2}$	=	mean-squared far-field acoustic pressure, Pa
p_ref	=	reference pressure, Pa
Re_c	=	chord-based Reynolds number
ρ	=	density, kg m^{-3}
St	=	Strouhal number
U_∞	=	free-stream velocity, m s^{-1}
K	=	permeability, m^2

*Corresponding Author, Ph.D Student, Aerodynamics, Wind Energy and Propulsion Dept., a.rubiocarpio@tudelft.nl, AIAA Student Member
†Assistant Professor, Aerodynamics, Wind Energy and Propulsion Dept., f.avallone@tudelft.nl
‡Assistant Professor, Aerodynamics, Wind Energy and Propulsion Dept., d.ragni@tudelft.nl
§Associate Professor, Control and Operations Dept., m.snellen@tudelft.nl
¶Professor, Aerospace Structures and Materials Dept., s.vanderzwaag@tudelft.nl

II. Introduction

Turbulent boundary layer trailing-edge (TBL-TE) noise is a major contributor to the overall broadband noise generated by modern wind turbines [1] and airframe noise for aircraft [2]. This aeroacoustic noise source has been subjected to research during the past decades to gain physical understanding and eventually find efficient noise control methods. TBL-TE noise is produced by a turbulent boundary layer convecting over the trailing edge of a lifting device [3]; accordingly, TBL-TE noise reduction approaches aim either at decreasing the energy content of turbulent structures and/or their spanwise coherence length at the trailing edge, or reducing the scattering efficiency of the surface discontinuity. Among others, serrations [4–6], brushes [7], finlets [8], aeroacoustic optimization of airfoil shape [9, 10] or boundary layer suction/blowing [11, 12] have been claimed as effective means to control TBL-TE noise, and some of them are currently being employed in the industry [13].

The application of permeable materials at the trailing edge also represents a promising TBL-TE noise abatement technique. Previous experiments report up to 11 dB noise reduction with respect to a reference (solid) case [14–16] for materials that establish flow communication between suction and pressure sides. This communication requirement could be fulfilled by applying homogeneous permeable materials with different micro-structures at the trailing edge: fiber felts [17], polyurethane foams [15], micro-perforated plates [18] or open-cell metal foams [19]. However, the permeability of most of these materials is altered, hence their capability to abate noise [20], when using conventional machining processes to shape them.

Recently developed manufacturing techniques such as 3D-printing [21] allow constructing permeable trailing edge inserts simply connecting suction and pressure sides of the airfoil with straight channels [22]. This possibility is specially interesting since it would allow to manufacture trailing edges with tailored permeability. Yet, it is important to determine if the differences in the internal structures of channeled and foam-based inserts play a role in their noise attenuation performance.

In the current manuscript, two different permeable trailing-edge designs are tested on a NACA 0018 at angles of attack α of 0 and 4.8° and chord-based Reynolds numbers Re_c of 3.4×10^5 and 5.4×10^5. The designs are based on the repetition of channels with axis normal to the chord, connecting suction and pressure sides of the trailing edge along the last 20% of the chord. The two perforated inserts have the same hole diameter d_h but different permeability K, obtained by varying the spacing between holes l_h. The noise scattering of the two perforated trailing edges, with an arranged micro-structure, are compared to that of open-cell metal foam inserts having different (random) micro-structure but similar permeability.

The current study is organized as follows. First, the experimental set-up, the 3D-printed inserts and the acoustic phased array are described in section III. Then, far-field noise measurements are discussed in section IV. Finally, in section V a summary of findings is given.

III. Experimental Set-up

A. Wind Tunnel and Model

The experimental investigation is performed in the anechoic vertical open-jet wind tunnel (A-Tunnel) of the Low Speed Laboratory (LSL) at Delft University of Technology. Experiments can be carried out at a maximum free-stream velocity of 45 m/s in the rectangular test section (40×70 cm^2). The turbulence intensity is below 0.1% and the streamwise velocity is uniform across the test section within 0.5% for all working conditions.

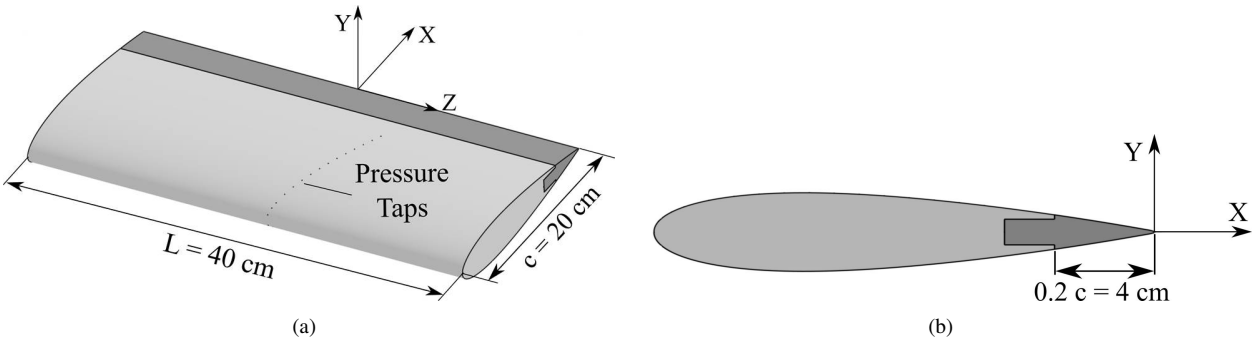

Fig. 1 Sketch of the NACA 0018 airfoil with 3D-printed insert. The aluminum body is represented in light grey while the insert appears in dark grey. (a) Perspective view. (b) Side view. Adapted from Rubio Carpio et al. [19]

The model, depicted in Fig. 1 (a), is a NACA0018 airfoil machined with Computer Numerical Control (surface roughness: 0.05 mm) using aluminium. The airfoil, with nominal chord length c = 20 cm and nominal span length L = 40 cm, is equipped with 30 pressure taps disposed at suction and pressure sides between 1 and 66% of the chord. The pressure taps are distributed within a plane inclined 15° with respect to the midspan plane of the airfoil to avoid disturbances in the measured pressure due to the wake of upstream cavities. The taps are connected to 15 *Honeywell* TruStability differential pressure sensors (range: -0.6 to 0.6 kPa; accuracy: 3 Pa) to measure static pressure data along the chord. The angle of attack α set at the experiment is assessed by comparison with the surface pressure distribution given by XFOIL [23]. As seen in Fig. 1(b), the airfoil can be retrofitted with trailing edge inserts manufactured with either solid or permeable materials. These inserts account for the last 20% of the chord (4 cm).

During the tests, the model is placed between two wooden side plates (Fig. 2 (a)) that guarantee the two-dimensionality of the flow. Boundary layer transition to turbulence is forced at 20% of the chord by means of a trip composed of 0.84 mm-height carborundum elements, randomly scattered along the span (Fig. 2 (b)). The turbulent state of the boundary layer is verified by an amplified stethoscope [24, 25], which discerns between the broadband signature of turbulent wall-pressure fluctuations and tonal or silent characteristic of laminar flows. The system is composed of a *Brüel & Kjaer* (B&K) 4134 microphone, a B&K 2619 preamplifier and a B&K 2801 power supply [26].

The streamwise-vertical-spanwise X-Y-Z coordinate system, also pictured in Fig. 1 (a) and (b), has its origin at the intersection between the midspan plane (Z = 0) and the trailing edge, and Y points at the microphone antenna; this system is employed in the remaining of the manuscript.

(a)

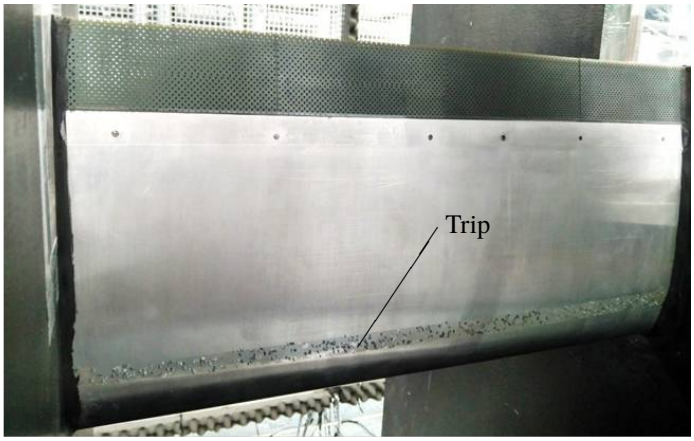

(b)

(c)

Fig. 2 (a) Overall view of the contraction with the airfoil and the side plates, and the microphone array on the back. (b) Detail view of the airfoil with a 3D-printed insert. (c) Detail of 3D-printed insert with l_h = 1.5 mm. Total length is 6 cm. Only the last 4 cm of insert are exposed to the flow.

B. 3D-printed Perforated Inserts

The perforated trailing-edge inserts are 3D-printed with an *EnvisionTEC*'s Perfactory 4 Standard (build envelope: 16×10×18 cm^3, resolution: 0.025 mm). The 6 cm-long perforated inserts are printed from root to tip using *EnvisionTEC*'s HTM 140 V2, a high-temperature molding material [27]. Due to the limited build envelope of the printer, 4 inserts with span length of 10 cm are assembled to build the entire trailing edge.

The inserts have cylindrical channels normal to the chord that connect suction and pressure side; these channels have a diameter d_h of 0.8 mm. The d_h is decreased to minimize low-frequency tones affecting the low-frequency part of the spectra [20].

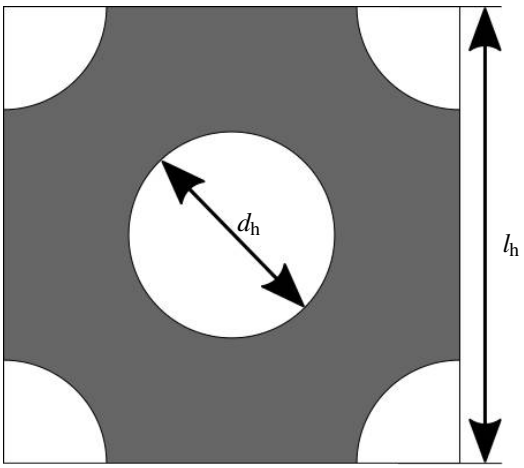

Fig. 3 Sketch of the hole pattern for perforated inserts.

The hole distribution is based on the repetition of the squared pattern [28] depicted in Fig. 3, where the hole spacing l_h controls the permeability K of the insert. Two different perforated inserts are studied in the present manuscript: one has a constant hole spacing of l_h = 1.5 mm, and the other has a l_h equal to 2.9 mm along 1.9 cm starting from the root, and l_h = 3 mm for the rest of insert.

The permeability K of the perforated inserts is obtained by measuring the static pressure drop Δp across perforated samples with same l_h as the inserts and thickness t = 10 mm, representative of the thickness of the trailing-edge insert (that varies from 15.7 mm at the root to 0.3 mm at the tip). The pressure drop across a sample of porous material is described by the Hazen-Dupuit-Darcy equation [29]

$$\frac{\Delta p}{t} = \frac{\mu}{K} v + \rho C v^2 \tag{1}$$

where ρ is the fluid density, μ is the dynamic viscosity, v is the Darcian velocity (defined as the ratio between the volumetric flow rate and the cross-section area of the sample) and K and C are the permeability and the form coefficient. These two parameters are obtained by least-squares fitting of Eq. (1) to 20 pressure drop data, measured for Darcian velocities ranging between 0 and 1.1 m/s [19, 30]. The porosity σ of the perforated inserts, defined as the ratio of empty-to-solid volume, is also computed as $\sigma = \pi d_h^2/(2l_h^2)$.

A summary of the characteristic parameters for perforated materials is presented in Table 1, where the resistivity $R = K/\mu$ is also reported for completeness. Since the noise scattering analysis includes a comparison with inserts manufactured with metal foams, a summary of their relevant parameters [30] is also included in Table 1.

Table 1 Characteristics of the permeable materials measured on samples with t = 0.01 m. P stands for perforated and MF stands for metal foam.

Type	d_c (mm)	d_h (mm)	l_h mm)	σ (-)	K (m^2)	R (Ns/m^4)	C (m^{-1})
P	-	0.8	3	0.105	1.5×10^{-9}	12050	8720
P	-	0.8	1.5	0.392	5.4×10^{-9}	3330	499
MF	0.45	-	-	0.893	0.5×10^{-9}	39970	11370
MF	0.58	-	-	0.905	1.7×10^{-9}	10730	3204

C. Acoustics Measurements

Far-field noise is measured with a planar phased microphone array containing 64 G.R.A.S. 40PH free-field microphones (frequency response: ±1 dB; frequency range: 10 Hz to 20 kHz; max. output: 135 dB ref. 20 μPa) with integrated CCP preamplifiers. As seen in Fig. 4, the microphone distribution corresponds to an adapted Underbrink design [31] with 7 spiral arms of 9 microphones each, and an additional microphone, with coordinates (X, Y, Z) = (-0.04, 1.02, 0) m, located at the center of the array. The array has spanwise and streamwise effective diameters of 1 and

2 m respectively. The measurements are performed on the suction side of the airfoil at a sample rate f_s of 50 kHz for 30 s. Analysis in the frequency domain is performed applying Fourier transform to data blocks with n_b = 5000 samples (T_b = 164 ms), yielding a frequency resolution $\Delta f = f_s/n_b$ equal to 10 Hz. To minimize spectral leakage, the blocks are windowed using a Hanning weighting function [32] with 50% data overlap.

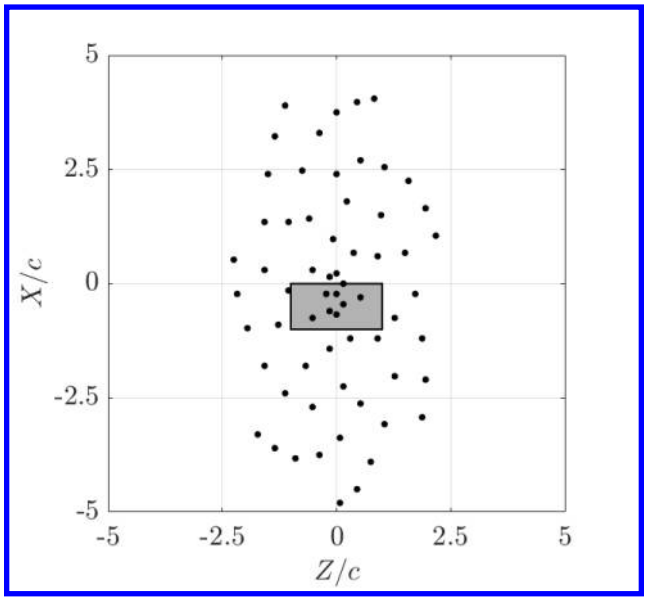

Fig. 4 Distribution of the microphones within the array. The position of the airfoil with respect to the array is marked by the grey area. The distance between the trailing edge and the microphone array plane d is 1.02 m.

To compute source maps, shown in Fig. 5 (a) and (b) for the baseline and the perforated insert with l_h = 3 mm case respectively, Conventional Frequency Domain Beamforming (CFDBF) [33] is applied to a square grid ranging between -2 < X/c < 2 and -2 < Z/c < 2 with 1 cm distance between grid points. The minimum distance at which the array can distinguish two sources R_c is given by the Rayleigh criterion [34] as $R_c = d\tan(1.22c_0/(fD))$, where c_0 refers to the speed of sound. The highest measured frequency in the present investigation (f_c = 3.15 kHz) yields a minimum distance R_c equal to 6 cm; hence, the space between grid points is 6 times smaller than the maximum resolution of the antenna. Due to the background noise levels encountered in the anechoic chamber for the described testing conditions, and the lower resolution of the array at low f, the minimum reported f_c is 500 Hz. The removal of acoustic sources other than broadband trailing edge noise is carried out applying source power integration [35] within -0.4 < Z/c < 0.4 and -0.6 < X/c < 0.4 (dashed rectangle in Fig. 5 (a) and (b)). Similar data processing yielded results with accuracy within 1 dB on synthetic data [36].

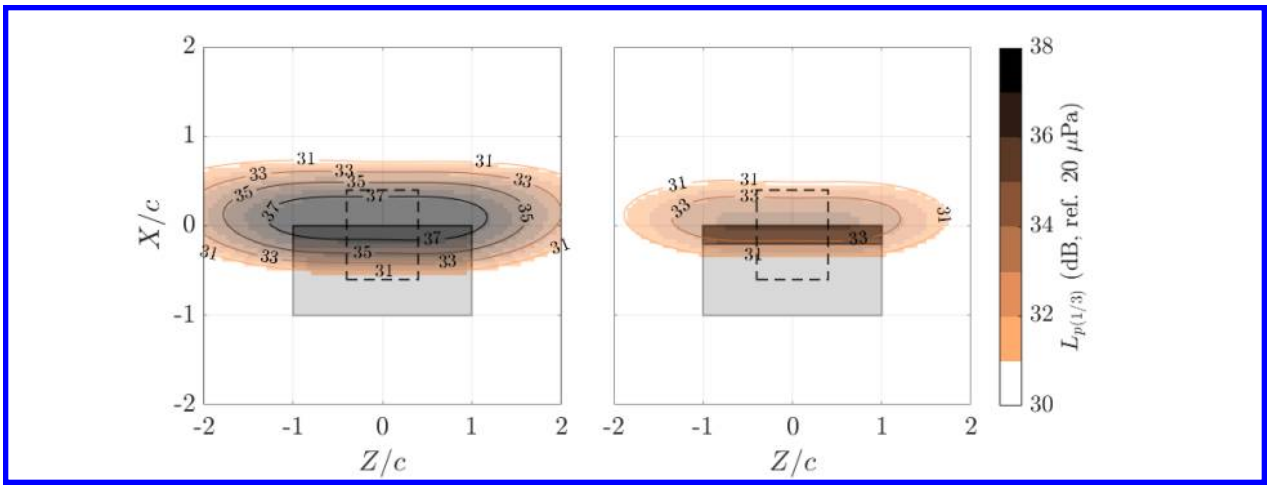

(a) (b)

Fig. 5 Source plots for the one-third octave band with f_c = 1600 Hz at U_∞ = 26 m/s. (a) Baseline. (b) Perforated with l_h = 3 mm. The airfoil is represented as a light grey rectangle. The perforated insert is depicted in dark grey. Dashed area represents the region where the source power integration technique is applied.

IV. Results

Noise scattering of the permeable inserts described in section III.B is evaluated through comparison with that of a fully solid one. Data are measured at free-stream velocities of 26 and 41 m/s (corresponding to chord-based Reynolds number of 3.4×10^5 and 5.4×10^5, respectively) and two angles of attack ($\alpha = 0°$ and 4.8°). To assess the validity of the measurements, data obtained at different free-stream velocities and no incidence for the reference case are presented in terms of Sound Pressure Level in one-third octave bands $L_{p\,(1/3)}$ as a function of the center frequencies f_c (Fig. 6 (a)) and scaled as follows:

$$L^*_{p\,(1/3)} = L_{p\,(1/3)} - m\log_{10}\left(\frac{U_\infty}{U_0}\right) \tag{2a}$$

$$\mathrm{St}_c = \frac{f_c c}{U_\infty} \tag{2b}$$

where U_0 = 1 m/s is a reference velocity, and m refers to the exponent for the scaling of far-field mean-squared acoustic pressure with free-stream velocity. In the present manuscript, m is computed through fitting the measured Overall Sound Pressure Level (OSPL) [37], calculated as

$$\mathrm{OSPL} = 10\ \log_{10}\sum_{f_c} 10^{L_{p(1/3)}/10} \tag{3}$$

to the free-stream velocity as OSPL = $m10\log_{10}(U_\infty) + b$, where b is an additional fit coefficient. For the baseline insert, the fit yields m = 5, in line with theoretical [4, 38] and experimental results [3] which predict m = 4.5 - 5. Data scaled using Eq. 2 (a) and (b) are depicted in Fig. 6 (b), where they collapse within 2 dB.

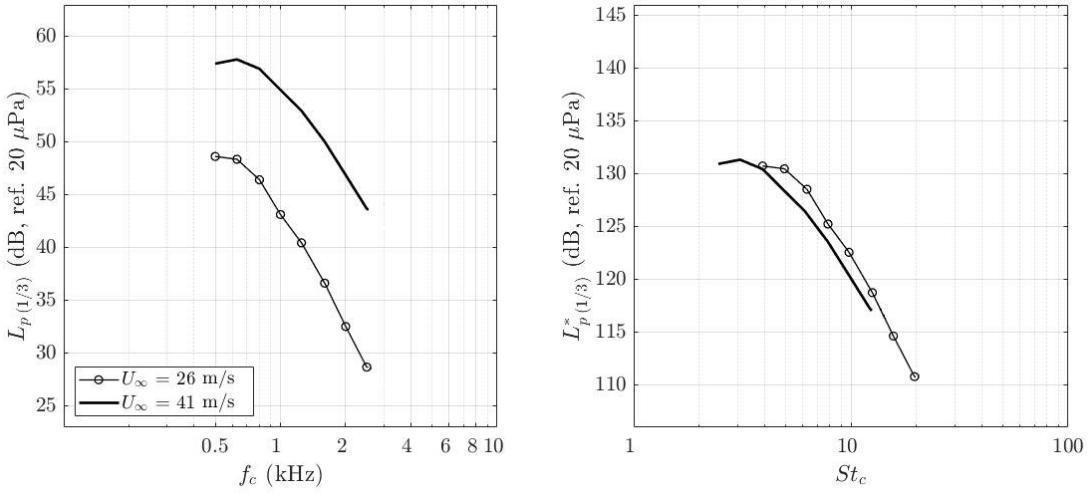

(a) (b)

Fig. 6 Far-field acoustic scattering for the baseline case (a) $L_{p\,(1/3)}$ for free stream velocities of 26 and 41 m/s and no incidence. (b) Collapse of measured data using the scaling described by Eq. 2(a) and (b)

The comparison of far-field noise scattered by the baseline and the permeable inserts is performed in terms of Sound Pressure Level in 1/3-octave bands $L_{p\,(1/3)}$. Data measured for all the trailing edge configurations described in section III.B are depicted in Fig. 7 (a) for U_∞ = 26 m/s and no incidence. To better illustrate noise reduction with respect to the baseline case, relative values $\Delta L_{p\,(1/3)} = L^{\text{solid}}_{p\,(1/3)} - L^{\text{perm.}}_{p\,(1/3)}$ are also shown in Fig. 7 (b), where positive values refer to noise abatement with respect to the baseline case. As reported previously [15, 39, 40], metallic foams reduce noise only below a material-dependent cross-over f_c. For the two metal foams used in the present study, namely d_c = 450 μm and d_c = 580 μm, the cross-over is respectively found at f_c = 2.5 and 2 kHz approximately. Below those frequencies, larger permeability yields higher maximum noise abatement levels [15]. Specifically, maximum noise reductions of 6 and 9 dB are measured for the d_c = 450 μm and d_c = 580 μm MF inserts. Above the cross-over frequency, MF inserts generate higher noise than the baseline case, with larger increase being measured for the MF with higher d_c. This contribution is generally attributed to the roughness of the material [20, 41, 42]. For the perforated trailing edges, similar features are reported: with the exception of the frequency band with f_c = 630 Hz -where the l_h = 1.5 mm insert generates a tonal noise- higher permeability produces larger maximum noise attenuation levels (5 and 9.5 dB for perforated inserts with l_h = 3 and 1.5 mm respectively). Furthermore, a cross-over f_c = 2.5 kHz is reported for the perforated edge with l_h = 3 mm. The most permeable perforated insert reported in the present manuscript (l_h = 1.5 mm) produces noise abatement (3 dB) at the highest reported frequency (f_c = 2.5 kHz). The $L_{p\,(1/3)}$ and $\Delta L_{p\,(1/3)}$ curves for the two perforated inserts have similar slopes -except for the tonal noise- thus suggesting a proportionality that is not present for MF inserts, where a cross-over between the two reported spectra occurs at f_c = 1 kHz approximately.

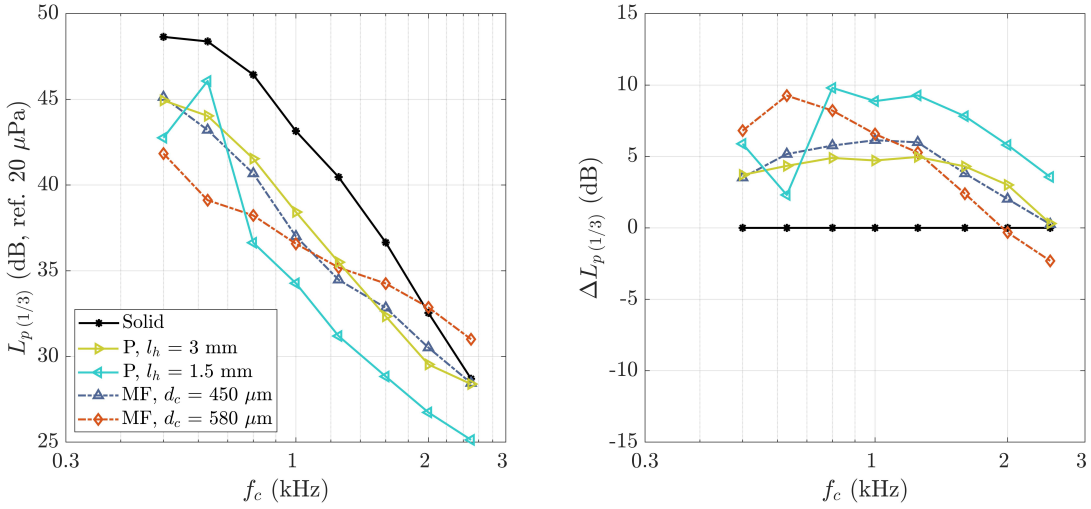

Fig. 7 Measured $L_{p\,(1/3)}$ for the permeable at solid inserts at U_∞ = 26 m/s and no incidence (a) Absolute values. (b) Relative values with respect to the solid insert.

Similar phenomena occur on data measured at incidence (α = 4.8°) at the same free-stream velocity, presented in Fig. 8 (a) and (b), in terms of absolute and relative $L_{p\,(1/3)}$. With this configuration, all the permeable inserts produce lower or similar broadband noise than the baseline case: the high-frequency excess noise discussed above is not measured for any of the investigated inserts. Maximum noise reduction levels are similar to those reported at no incidence: up to 4 and 7.5 dB noise reduction is measured for perforated inserts, and up to 4 and 7 dB for MF inserts with increasing permeability. It is also interesting to note that the tone reported for the most permeable perforated insert (l_h = 1.5 mm) at 0° within the frequency band with f_c = 630 Hz is not visible at incidence. For these testing conditions, the previously reported similarity between the slope of spectra for the perforated inserts is also observed; while the cross-over frequency between MF inserts is once more reported at approximately f_c = 1 kHz.

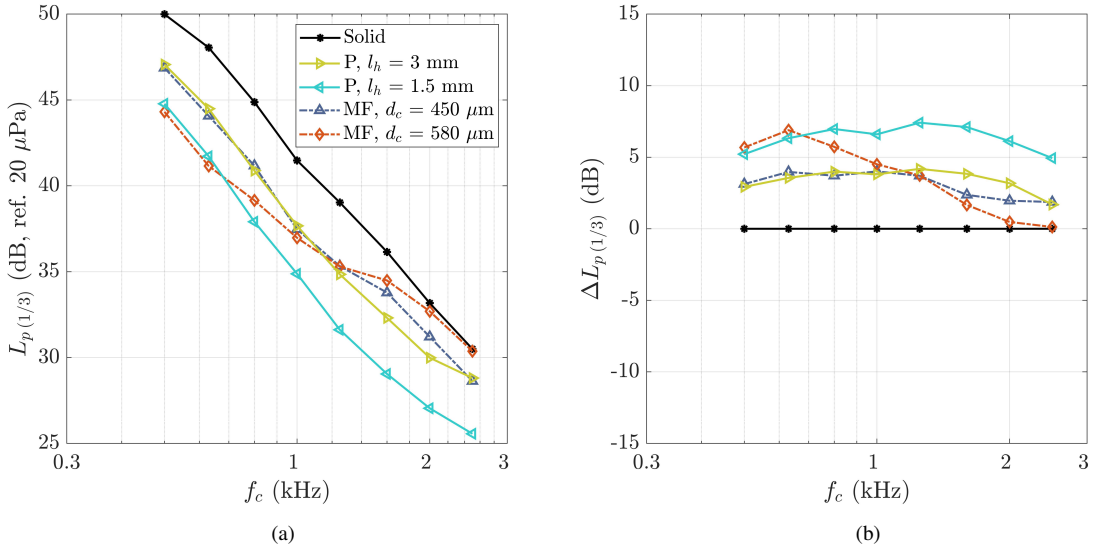

Fig. 8 Measured $L_{p\,(1/3)}$ for the permeable at solid inserts at U_∞ = 26 m/s and α = 4.8° (a) Absolute values. (b) Relative values with respect to the solid insert.

The change in OSPL with free-stream velocity, shown in Fig. 9 (a) and (b) for α = 0° and α = 4.8°, is evaluated. To

assess the change in far-field acoustic pressure with velocity, the fit to an exponent m described at the beginning of the section is applied to data measured for permeable inserts. Results corresponding to the perforated insert with l_h = 1.5 mm are not shown, since they are strongly affected by the previously described tone. At no incidence, the analysis shows that for permeable inserts the OSPL scales with exponents of the free-stream velocity larger than those of the baseline case. This is in agreement with the analytical solution for a semi-infinite flat plate with porous extension [43], that yields an increase from m = 5 (solid plate) to m = 6. In Fig. 9 (a), it is observed that MF inserts increase m from 5.5 to 6.1 for increasing permeability/cell diameter values. An increase up to m = 7 is also reported in Geyer et al. [17] for MF inserts applied to a chambered airfoil. The fitting coefficient for the perforated edge (m = 5.3) is similar to that of the MF insert with d_c = 450 μm. Additionally, in Fig. 9 (b) the scaling for these two inserts for data measured at lifting conditions yield similar values. As shown in Table 1, for a given noise reduction level, they have significantly different permeability (the perforated design is three times as permeable as the MF). Hence, the permeability of an insert can be considered as a good indicator of the noise attenuation performance, but it is insufficient to fully characterize the noise scattering of trailing-edge inserts with significantly different micro structures.

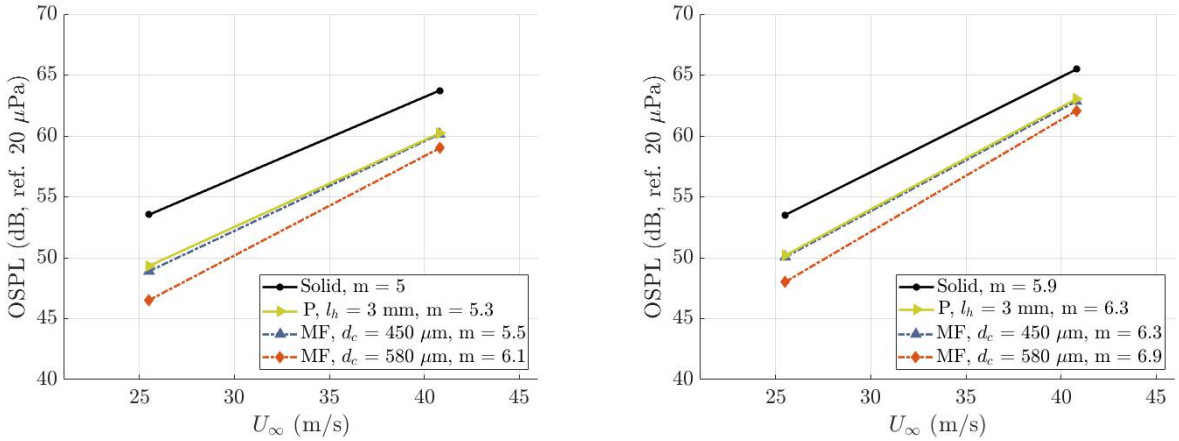

Fig. 9 Change of OSPL with free-stream velocity for the permeable and solid inserts. (a) α = 0°. (b) α = 4.8°.

This consideration is detailed in Fig. 10, where the reduction in OSPL with respect to the solid case ΔOSPL = $OSPL^{solid}$ - $OSPL^{perm.}$ is plotted as a function of the permeability of the inserts. For the sake of conciseness, only results measured at U_∞ = 26 m/s are presented (data measured at U_∞ = 41 m/s yield similar conclusions). For the reason explained above, results corresponding to the perforated insert with permeability of 5.4×10^{-9} m^2 are only reported at incidence. Increase in noise abatement for materials with larger permeability is exclusively measured within inserts with similar pore arrangement. It is also observed that, to achieve similar noise attenuation levels, the perforated inserts must be at least three times as permeable as the MF inserts: up to 5 dB noise reduction can be obtained employing MF treatments with permeability of 0.5×10^{-9} m^2 or perforated inserts with permeability of 1.5×10^{-9} m^2; similarly, larger noise attenuation levels -between 5.5 and 6 dB- are measured for both the metal foam with permeability of 1.7×10^{-9} m^2 and the perforated edge with permeability of 5.4×10^{-9} m^2. Similarly, inserts with comparable permeability -between 1.5×10^{-9} and 1.7×10^{-9} m^2- produce remarkably different noise attenuation levels (up to 3 dB difference) depending on the type of insert -perforated or metal foam- both for zero and 4.8° incidence; interestingly, for these inserts the random micro-structure performs better than the arranged pore distribution.

In view of the present results, other material parameters describing the different pore organization of permeable materials, such as tortuosity [44], seem necessary to fully characterize their noise scattering. This property would account for additional energy dissipation through viscous effects within the porous material, which might increase noise abatement. The change in the noise abatement with inserts with different pore organization for a given permeability will be further addressed in the future.

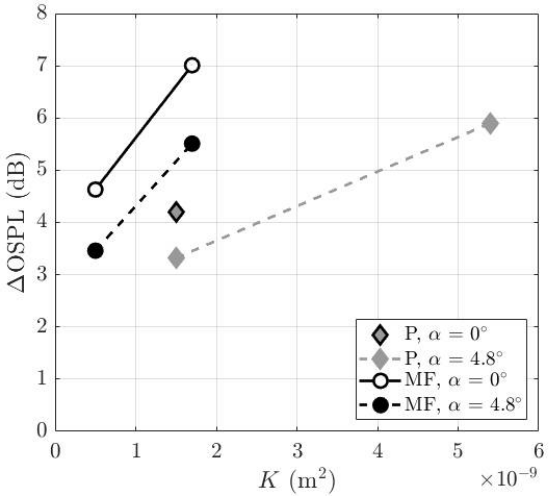

Fig. 10 Decrease in OSPL with respect to the solid configuration for metal foam (MF) and perforated (P) inserts with different permeability K at U_∞ = 26 m/s.

V. Conclusions

Measurements of the far-field noise scattered by a NACA0018 airfoil retrofitted with solid and 3D-printed permeable trailing-edge inserts installed in the last 20% of the chord are performed. The inserts have straight passages perpendicular to the chord that communicate the suction and pressure side of the trailing edge. A channel diameter of 0.8 mm is employed for the two inserts, and their permeability is controlled by changing the distance between holes from 1.5 to 3 mm, yielding permeability values of 1.5 and 5.4 $\times 10^{-9}$ m^2. To assess the effect of the pore distribution within the insert, noise scattering for perforated inserts is compared to that of permeable inserts manufactured with materials with random micro-structure (metallic foams). The experiments are performed at free-stream velocities of 26 and 41 m/s, corresponding to chord-based Reynolds numbers of 3.4×10^5 and 5.4×10^5, and angles of attack of 0 and 4.8°.

Far-field noise spectra measured with a planar microphone antenna show that, similarly to other permeable materials, larger broadband noise attenuation levels are measured for the perforated edge with higher permeability regardless of the lifting condition. It is observed that, in order to obtain similar broadband noise attenuation levels, the 3D-printed inserts must be at least 3 times as permeable as the metal foam ones. Similarly, for comparable permeability values (between 1.5 and 1.7 $\times 10^{-9}$ m^2), the metal foam insert outperforms the perforated one in all measured lifting conditions. It is thus concluded that noise abatement (both in absolute values and in the frequency range over which noise reduction is observed) is not fully determined by the permeability of the inserts. Hence, additional parameters accounting for the micro-structural complexity of permeable materials should be considered in future research.

References

[1] Oerlemans, S., Sijtsma, P., and Méndez López, B. ., "Location and quantification of noise sources on a wind turbine," *Journal of Sound and Vibration*, 2007. doi:10.1016/j.jsv.2006.07.032.

[2] Casalino, D., Diozzi, F., Sannino, R., and Paonessa, A., "Aircraft noise reduction technologies: A bibliographic review," *Aerospace Science and Technology*, Vol. 12, No. 1, 2008, pp. 1–17. doi:10.1016/j.ast.2007.10.004.

[3] Brooks, T. F., Pope, D. S., and Marcolini, M. A., "Airfoil self-noise and prediction," Tech. rep., NASA Langley Research Center, 1989.

[4] Howe, M. S., "Aerodynamic noise of a serrated trailing edge," *Journal of Fluids and Structures*, Vol. 5, No. 1, 1991, pp. 33–45. doi:10.1016/0889-9746(91)80010-B.

[5] Chong, T. P., and Vathylakis, A., "On the aeroacoustic and flow structures developed on a flat plate with a serrated sawtooth trailing edge," *Journal of Sound and Vibration*, Vol. 354, 2015, pp. 65–90. doi:10.1016/j.jsv.2015.05.019.

[6] Avallone, F., van der Velden, W. C. P., and Ragni, D., "Benefits of curved serrations on broadband trailing-edge noise reduction," *Journal of Sound and Vibration*, Vol. 400, 2017, pp. 167–177. doi:10.1016/j.jsv.2017.04.007.

[7] Finez, A., Jacob, M., Jondeau, E., and Roger, M., "Broadband Noise Reduction with Trailing Edge Brushes," *16th AIAA/CEAS Aeroacoustics Conference*, 2010, pp. 1–13. doi:10.2514/6.2010-3980.

[8] Clark, I. A., Daly, C. A., Devenport, W., Alexander, W. N., Peake, N., Jaworski, J. W., and Glegg, S., "Bio-inspired canopies for the reduction of roughness noise," *Journal of Sound and Vibration*, Vol. 385, 2016, pp. 33–54. doi:10.1016/j.jsv.2016.08.027.

[9] Mardsen, A. L., Wang, M., Dennis, J. E., and Moin., P., "Trailing Edge Noise Reduction Using Derivative-free Optimization And Large Eddy Simulation," *Journal of Fluid Mechanics*, 2007. doi:10.1017/S0022112006003235.

[10] Jones, R. F., Doolan, C. J., and Teubner, M. D., "Minimization of trailing edge noise by parametric airfoil shape modifications," *17th AIAA/CEAS Aeroacoustics Conference*, 2011, pp. 1–16. doi:10.2514/6.2011-2782.

[11] Gerhard, T., Erbslöh, S., and Carolus, T., "Reduction of airfoil trailing edge noise by trailing edge blowing," *Journal of Physics: Conference Series*, Vol. 524, No. 1, 2014. doi:10.1088/1742-6596/524/1/012123.

[12] Arnold, B., Rautmann, C., Lutz, T., and Kraemer, E., "Design of a boundary-layer suction system for trailing-edge noise reduction of an industrial wind turbine," *35th Wind Energy Symposium*, American Institute of Aeronautics and Astronautics, 2017, pp. 1–15. doi:10.2514/6.2017-1380.

[13] Oerlemans, S., "Reduction of wind turbine noise using blade trailing edge devices," *22nd AIAA/CEAS Aeroacoustics Conference*, 2016, pp. 1–18. doi:10.2514/6.2016-3018.

[14] Geyer, T., and Sarradj, E., "Noise generation by porous airfoils," *13th AIAA/CEAS Aeroacoustics Conference*, 2007. doi:10.2514/6.2007-3719.

[15] Geyer, T., and Sarradj, E., "Trailing edge noise of partially porous airfoils," *20th AIAA/CEAS Aeroacoustics Conference*, 2014. doi:10.2514/6.2014-3039.

[16] Rubio Carpio, A., Merino Martínez, R., Avallone, F., Ragni, D., Snellen, M., and van der Zwaag, S., "Experimental characterization of the turbulent boundary layer over a porous trailing edge for noise abatement," *Journal of Sound and Vibration*, Vol. 443, 2019, pp. 537–558. doi:10.1016/j.jsv.2018.12.010, URL `https://linkinghub.elsevier.com/retrieve/pii/S0022460X18308277`.

[17] Geyer, T., Sarradj, E., and Fritzsche, C., "Porous airfoils: noise reduction and boundary layer effects," *International Journal of Aeroacoustics*, Vol. 9, No. 6, 2010, pp. 787–820. doi:10.1260/1475-472x.9.6.787.

[18] Herr, M., and Reichenberger, J., "In Search of Airworthy Trailing-Edge Noise Reduction Means," *17th AIAA/CEAS Aeroacoustics Conference*, 2011, pp. 5–8. doi:10.2514/6.2011-2780.

[19] Rubio Carpio, A., Avallone, F., and Ragni, D., "On the role of the flow permeability of metal foams on trailing edge noise reduction," *2018 AIAA/CEAS Aeroacoustics Conference*, American Institute of Aeronautics and Astronautics, 2018, pp. 1–18. doi:10.2514/6.2018-2964.

[20] Herr, M., Rossignol, K. S., Delfs, J., Lippitz, N., and Moßner, M., "Specification of Porous Materials for Low-Noise Trailing-Edge Applications," *20th AIAA/CEAS Aeroacoustics Conference*, 2014, pp. 1–19. doi:10.2514/6.2014-3041.

[21] Gibson, I., Rosen, D., and Stucker, B., *Additive Manufacturing Technologies*, Springer New York, New York, NY, 2015. doi:10.1007/978-1-4939-2113-3.

[22] Jiang, C., Moreau, D., Yauwenas, Y., Fischer, J. R., Doolan, C. J., Gao, J., Jiang, W., McKay, R., and Kingan, M., "Control of rotor trailing edge noise using porous additively manufactured blades," *2018 AIAA/CEAS Aeroacoustics Conference*, American Institute of Aeronautics and Astronautics, Reston, Virginia, 2018. doi:10.2514/6.2018-3792.

[23] Drela, M., "XFOIL: an analysis and design system for low Reynolds number airfoils," *Low Reynolds Number Aerodynamics: Proceedings of the Conference Notre Dame, Indiana, USA, 5–7 June 1989*, Springer Berlin Heidelberg, Berlin, Heidelberg, 1989, pp. 1–12. doi:10.1007/978-3-642-84010-4{_}1.

[24] Butler, S. F. J., "Current tests on laminar-boundary-layer control by suction through perforations," *Aeronautical Research Council Reports and Memoranda*, Vol. 3040, No. 3040, 1957.

[25] Gooden, J. H. M., "Experimental low-speed aerodynamic characteristics of the Wortmann FX66-S-196 V1 airfoil," *XVI OSTIV Congress*, Chateauroux, France, 1978, pp. 1–11.

[26] Lentink, D., and de Kat, R., "Gliding Swifts Attain Laminar Flow over Rough Wings," *PLoS ONE*, Vol. 9, No. 6, 2014, p. e99901. doi:10.1371/journal.pone.0099901.

[27] EnvisionTEC GmbH, "Htm 140 V2 Technical Datasheet," , 2018. URL https://envisiontec.com/wp-content/uploads/2016/09/2018-HTM-140-V2-1.pdf.

[28] Bae, Y., and Kim, Y. I., "Numerical modeling of anisotropic drag for a perforated plate with cylindrical holes," *Chemical Engineering Science*, Vol. 149, 2016, pp. 78–87. doi:10.1016/j.ces.2016.04.036, URL http://dx.doi.org/10.1016/j.ces.2016.04.036.

[29] Ingham, D., and Pop, I., *Transport phenomena in porous media*, Pergamon, 1998.

[30] Rubio Carpio, A., Merino-Martínez, R., Avallone, F., Ragni, D., Snellen, M., and van der Zwaag, S., "Broadband trailing edge noise reduction using permeable metal foams," *46th International Congress and Exposition of Noise Control Engineering, 27–30 August, 2017, Hong Kong*, 2017, pp. 4373–4383.

[31] Luesutthiviboon, S., Malgoezar, A., Snellen, M., Sijtsma, P., and Simons, D., "Improving Source Discrimination Performance by Using an Optimized Acoustic Array and Adaptive High-Resolution CLEAN-SC Beamforming," *7th Berlin Beamforming Conference*, 2018.

[32] Brandt, A., *Noise and vibration analysis: signal analysis and experimental procedures*, John Wiley & Sons, ltd, 2011. doi:10.1002/9780470978160.

[33] Mueller, T. J., *Aeroacoustic measurements*, Berlin New York Springer, 2002. doi:10.1007/978-3-662-05058-3.

[34] Rayleigh, L., "Investigations in optics, with special reference to the spectroscope," *Philosophical Magazine Series 5*, Vol. 8, No. 49, 1879, pp. 261–274. doi:10.1080/14786447908639684.

[35] Merino-Martínez, R., Sijtsma, P., and Snellen, M., "Inverse Integration Method for Distributed Sound Sources," *7th Berlin Beamforming Conference*, 2018, pp. 1–21.

[36] Sarradj, E., Herold, G., Sijtsma, P., Merino Martínez, R., Geyer, T., Bahr, C. J., Porteous, R., Moreau, D., and Doolan, C. J., "A Microphone Array Method Benchmarking Exercise using Synthesized Input Data," *23rd AIAA/CEAS Aeroacoustics Conference*, 2017, pp. 1–16. doi:10.2514/6.2017-3719.

[37] Moore, B., *Hearing*, Elsevier Science, 1995.

[38] Ffowcs-Williams, J. E., and Hall, L. H., "Aerodynamic sound generation by turbulent flow in the vicinity of a scattering half plane," *Journal of Fluid Mechanics*, Vol. 40, No. 04, 1970, p. 657. doi:10.1017/s0022112070000368.

[39] Geyer, T., Sarradj, E., and Fritzsche, C., "Measurement of the noise generation at the trailing edge of porous airfoils," *Experiments in Fluids*, Vol. 48, No. 2, 2010, pp. 291–308. doi:10.1007/s00348-009-0739-x.

[40] Rubio Carpio, A., Merino-Martínez, R., Avallone, F., Ragni, D., Snellen, M., and van der Zwaag, S., "Experimental characterization of the turbulent boundary layer over a porous trailing edge for noise abatement," *Journal of Sound and Vibration*, 2018.

[41] Geyer, T., Sarradj, E., and Fritzsche, C., "Porous airfoils: noise reduction and boundary layer effects," *15th AIAA/CEAS Aeroacoustics Conference*, American Institute of Aeronautics and Astronautics, 2009. doi:10.2514/6.2009-3392.

[42] Rubio Carpio, A., Avallone, F., and Ragni, D., "On the role of the flow permeability of metal foams on trailing edge noise reduction," *2018 AIAA/CEAS Aeroacoustics Conference*, 2018. doi:10.2514/6.2018-2964.

[43] Jaworski, J. W., and Peake, N., "Aerodynamic noise from a poroelastic edge with implications for the silent flight of owls," *Journal of Fluid Mechanics*, Vol. 723, No. 2013, 2013, pp. 456–479. doi:10.1017/jfm.2013.139.

[44] Epstein, N., "On tortuosity and the tortuosity factor in flow and diffusion through porous media," *Chemical Engineering Science*, Vol. 44, No. 3, 1989, pp. 777–779. doi:10.1016/0009-2509(89)85053-5, URL http://linkinghub.elsevier.com/retrieve/pii/0009250989850535.